

# Sound-Based Analogue of Cavity Quantum Electrodynamics in Silicon

Ö. O. Soykal, Rusko Ruskov, and Charles Tahan

Laboratory for Physical Sciences, 8050 Greenmead Dr., College Park, MD 20740

A quantum mechanical superposition of a long-lived, localized phonon and a matter excitation is described. We identify a realization in strained silicon: a low-lying donor transition (P or Li) driven solely by acoustic phonons at wavelengths where high- $Q$  phonon cavities can be built. This phonon-matter resonance is shown to enter the strongly-coupled regime where the “vacuum” Rabi frequency exceeds the spontaneous phonon emission into non-cavity modes, phonon leakage from the cavity, and phonon anharmonicity and scattering. We introduce a micropillar distributed Bragg reflector Si/Ge cavity, where  $Q \simeq 10^5 - 10^6$  and mode volumes  $\mathcal{V} \lesssim 25\lambda^3$  are reachable. These results indicate that single or many-body devices based on these systems are experimentally realizable.

Cavity-quantum electrodynamics (cQED) refers to the interaction of a single-mode of the electromagnetic field with a dipole emitter. cQED has provided new ways of controlling photons and matter (atoms, qubits, etc.) in both atomic and solid-state systems. The progression from an atom “dressed” with a cavity photon (“traditional” cavity-QED) [1, 2] to a semiconductor microcavity-polariton (exciton plus cavity-photon) [3] to solid-state many-body polaritonic devices [4, 5, 9] has opened up new avenues for physical investigation as well as technology (e.g., single photon sources, novel lasers, long-range entanglement, quantum simulation). Motivated by this, we seek an analogous progression utilizing quantum sound instead of light.

Phonons are more suitable for some tasks than photons due to their slower speeds and smaller wavelengths (e.g., in signal processing, sensing, or nanoscale imaging). Our work builds off recent experimental results in nano-optomechanical systems [7], where cooling, coherent control, and lasing of mechanical vibrations has been achieved, as well as previous consideration of phonons as decoherence pathways [8], as tools for coupling quantum systems [9–11], and even as a means for simulating many-body dynamics [12].

In this Letter, we show that a phonon-based analogue of the cavity-polariton is possible. Introducing a suitable high- $Q$  phonon cavity, we calculate the cavity phonon coupling to a two-level system (TLS) in silicon (Fig. 1) and also losses due to spontaneous phonon emission from the donor into non-cavity modes, phonon leakage from the cavity, and phonon anharmonicity and scattering. Despite the phonon’s dependent nature on its host material and the different (non-dipole) donor/phonon interaction, a strong coupling regime can be established, similar to cQED, where the phonon-TLS states are hybridized. The result of this mixing of cavity-phonon and matter excitation we term the cavity-*phoniton* [13].

*Implementation.* Silicon is a promising candidate for constructing a cavity-phoniton system. The physics of shallow donors in Si have been understood since 1950s and experimentally verified, while transitions between low energy donor states are known to be driven by acous-

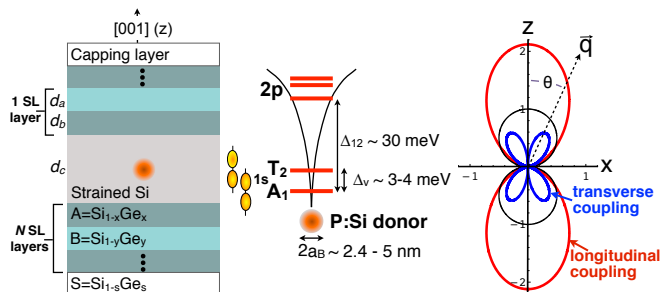


Figure 1. (a) A cavity-phoniton can be constructed in a Si/Ge heterostructure cavity as a hybridized state of a trapped single phonon mode and a donor TLS placed at a maxima of the phonon field. (b) The P:Si donor lowest  $1s$  valley states,  $A_1$ ,  $T_2$ , and upper levels ( $1s/2p$ ); their energy splittings can be controlled by the applied strain in the Si cavity. (c) Angular dependence of the coupling  $g_q(\theta)$ , Eq.(2), for the deformation potentials of Ref. [15] vs. dipole  $\sim \cos \theta$  dependence (thin circles).

tic phonons [5]. The six-fold degeneracy due to Si’s multi-valley conduction band is lifted both by applied strain (e.g., due to the lattice mismatch with a substrate) and the sharp donor potential. Crucially, in [001] compressively strained-Si (Fig. 1), the first excited state at zero magnetic field of a phosphorous donor approaches  $\Delta_v^P \simeq 3.02$  meV (0.73 THz): a so-called excited “valley” state. (The excited valley state has an  $s$ -like envelope function like the ground state but opposite parity; because of this, valley state relaxation times can be much longer than for charge states). The energy splitting implies longitudinal (transverse) wavelengths of  $\lambda_l \approx 12.3$  nm ( $\lambda_t \approx 7.4$  nm). For comparison, the energy splitting to the upper  $2p$ -like state is  $> 30$  meV ( $\lambda_{2p} \approx 1.2$  nm), unlikely to be amenable to phonon cavities. Since the P:Si Bohr radius is  $a_B^* \lesssim 2.5$  nm in the bulk,  $\lambda > a_B^*$  allows for easier donor placement, avoidance of interface physics, and bulk-like wave functions.

A prototype implementation of a cavity-phoniton system in silicon is sketched in Fig. 1a. A strained-Si phonon cavity grown in the [001] direction, of length  $d_c \sim \lambda$  and lateral size  $D$ , is enclosed by acoustic DBRs formed as layered, epitaxially-grown, and strain-relaxed SiGe super

lattice (SL) heterostructures. The cavity length is chosen to be less than the critical thickness due to strain (see, e.g., Ref. [10]). The DBR SL unit periods consist of subsequent layers  $(A, B) = \text{Si}_{1-x_{A,B}}\text{Ge}_{x_{A,B}}$  of thickness  $(d_A, d_B)$ , strain matched to a  $\text{Si}_{1-s}\text{Ge}_s$  substrate ( $x_{A(B)} = 0.55(0.05)$ ,  $s = 0.26$ , maximizing confinement) and an appropriate capping layer, depending on the actually confined phonon mode. Note that 1D DBR SL phonon cavities ( $D \gg d_c$ ) are well understood and have been demonstrated in THz phonon cavities in III-Vs [7, 13]; coherent phonons in SiGe superlattices were studied as well [20]. In the case of micropillar DBR (mpDBR) structures (designed to increase the phonon-donor coupling), the DBR lateral dimension may become comparable to the phonon wavelength ( $D \gtrsim d_c \sim \lambda$ ) and the confined mode is a mixed longitudinal/transverse one. The trapped mode with wavelength  $\lambda_q$  and phase velocity  $v_q$  is designed to be resonant in energy with the first excited state of the donor. Similar to the 1D DBR [8], the thickness of the SL unit cell is set to match the Bragg condition  $d_{A,B}^{(q)} = v_{A,B}^{(q)} \lambda_q / 4v_q$ , where  $v_{A,B}^{(q)}$  are the phase velocities (using isotropic approximation, see, e.g., Ref. [23]). The donor is placed at the center of a  $\lambda$ -cavity ( $d_c = \lambda_q$ ), where the displacement  $\mathbf{u}(\mathbf{r})$  is maximal [24].

*Hamiltonian and coupling.* In the semi-classical picture an acoustic phonon creates a time-dependent strain,  $\varepsilon_{\alpha\beta}(\mathbf{r}) = \frac{1}{2} \left( \frac{\partial u_\alpha}{\partial r_\beta} + \frac{\partial u_\beta}{\partial r_\alpha} \right)$ , which modulates the energy bands and can drive transitions in a localized state, e.g., a donor. For Si, from the multivalley electron-phonon interaction [2, 15] one can derive the matrix element between valley states,  $|s, j\rangle$ :

$$V_{ij}^{s's} \equiv \hbar g_{\mathbf{q}} = i \langle s', i | \Xi_d \text{Tr}(\varepsilon_{\alpha\beta}) + \frac{1}{2} \Xi_u \left\{ \hat{\mathbf{k}}_i^\alpha \hat{\mathbf{k}}_i^\beta + \hat{\mathbf{k}}_j^\alpha \hat{\mathbf{k}}_j^\beta \right\} \varepsilon_{\alpha\beta} |s, j\rangle, \quad (1)$$

where  $\hat{\mathbf{k}}_{i,j}$  are the directions toward the valleys,  $s, s'$  label the orbital (envelope) function(s), and  $\Xi_u(\text{Si}) \simeq 8.77 \text{ eV}$ ,  $\Xi_d(\text{Si}) \approx 5 \text{ eV}$  [15] are deformation potential constants. For the donor-phonon Hamiltonian we obtain the interaction (of Jaynes-Cummings type):  $H_g \approx \hbar g_{\mathbf{q}} (\sigma_{ge}^+ b_{\mathbf{q},\sigma} + \sigma_{ge}^- b_{\mathbf{q},\sigma}^\dagger)$  where only the resonant cavity phonon with quantum numbers  $\mathbf{q}, \sigma$  and energy  $\hbar\omega_{\mathbf{q},\sigma}$  is retained,  $b_{\mathbf{q},\sigma}^\dagger$  is the phonon creation operator, and  $\sigma_{ge}^+ \equiv |e\rangle\langle g|$  refers to the donor transition between ground and excited states. In the loss part:  $H_{\text{loss}} = H_\kappa + H'_{\text{anh}} + H_\Gamma$ ,  $H_\kappa$  couples the cavity mode to external continuum of other modes giving a cavity decay rate  $\kappa = \omega_{\mathbf{q},\sigma}/Q$  (expressed through the  $Q$ -factor);  $H'_{\text{anh}}$  includes phonon decay due to phonon self-interaction and also phonon scattering off impurities (mainly mass fluctuations in natural Si). The coupling of the donor to modes other than the cavity mode,  $H_\Gamma$ , leads to its spontaneous decay.

The valley states:  $1s(A_1)$ ,  $1s(T_2)$ , that make up the TLS are the symmetric and anti-symmetric combinations of the conduction band valley minima along the

$\hat{z}$ -direction (see Fig. 1b). Due to opposite parity of the states the intravalley contributions cancel. The intervalley transitions are preferentially driven by Umklapp phonons [6] with a wave vector  $\mathbf{q}$  at  $q_u \simeq 0.3 \frac{2\pi}{a_0}$ , where  $\mathbf{q}_u \equiv \mathbf{G}_{+1} - 2\mathbf{k}_z$  is the wave vector ‘‘deficiency’’ of the intervalley  $\mathbf{k}_z \rightarrow -\mathbf{k}_z$  transition, and  $\mathbf{G}_{+1} = \frac{4\pi}{a_0}(0, 0, 1)$  is the reciprocal vector along  $\hat{z}$ . Since typical values give  $q_u r \approx q_u a_B^* \simeq 9.4 > 1$  and  $qr \sim 1$  for 3 meV, the coupling is calculated exactly (not using the dipole approximation) for longitudinal and transverse polarizations

$$g_{\mathbf{q}}^{(\sigma)} = \left( \frac{a_G^2 q^2}{2\rho\hbar\mathcal{V}\omega_{\mathbf{q},\lambda}} \right)^{1/2} I^{ge}(\theta) \begin{cases} \Xi_d + \Xi_u \cos^2\theta & [l] \\ \Xi_u \sin\theta \cos\theta & [t] \end{cases}, \quad (2)$$

where  $a_G \approx 0.3$ ,  $I^{ge}(\theta) = \int d\mathbf{r} [\Phi_{1s}^z(\mathbf{r})]^2 e^{-i\mathbf{q}\mathbf{r}} \sin(\mathbf{q}\mathbf{r}) = \frac{2\beta_q \cos\theta (1-\gamma_q \cos^2\theta)}{\alpha_q^2 [(1-\gamma_q \cos^2\theta)^2 - \beta_q^2 \cos^2\theta]^2}$  is the intervalley overlapping factor,  $\alpha_q = 1 + \frac{1}{4}(q^2 a^2 + q_u^2 b^2)$ ,  $\beta_q = \frac{1}{2\alpha_q} b^2 q q_u$ ,  $\gamma_q = \frac{1}{4\alpha_q} (a^2 - b^2) q^2$ , and  $a/b$  are the radii of the Kohn-Luttinger envelope function  $\Phi_{1s}^z(\mathbf{r})$  (see, e.g. Ref.[15]). The calculated coupling is to plane wave modes, related to a rectangular cavity with periodic boundary conditions. Fig. 1c shows the directionality of the coupling for longitudinal and transverse phonons. The angular dependence in Eq. (2) for longitudinal phonons is similar to dipole emission ( $I_{\text{dip}}^{ge} \sim \cos\theta$ ), but enhanced in a cone around  $\hat{z}$ -direction due to non-dipole contributions. Uncertainties in  $\Xi_d$  calculations (see Ref. [25]) result in an overall factor of 2 difference in the maximal coupling.

*Coupling to cavity mode.* The matrix element  $\hbar g_{\mathbf{q}}^{(\sigma)}$  is just the interaction energy of the donor with the ‘‘phonon vacuum field’’ and expresses a generic dependence  $\propto 1/\sqrt{\mathcal{V}}$  on the normalization volume; it goes to zero for large volumes. In a cavity,  $\mathcal{V}$  is the physical volume of the mode [3]. By virtue of Eq. (2), we first consider a DBR cavity with a length  $d_c = \lambda_l \simeq 12.3 \text{ nm}$  designed for longitudinal resonant phonon along the  $z$ -direction (we use isotropic velocities for Si:  $v_l = 8.99 \cdot 10^3 \text{ m s}^{-1}$ ,  $v_t = 5.4 \cdot 10^3 \text{ m s}^{-1}$ , see Ref.[23]). Taking the minimal lateral size  $D_{\text{min}} \approx \lambda_l$  to ensure  $D > 2a_B^* \approx 5 \text{ nm}$ , one gets a mode volume of  $\mathcal{V}_{\text{min}} \approx \lambda^3$  for P:Si. Thus, we estimate the maximal phonon-donor coupling as  $g_{1\lambda} = 3.7 \cdot 10^9 \text{ s}^{-1}$ . For  $D = 5\lambda$  the coupling is still appreciable:  $g_{5\lambda} = 7.4 \cdot 10^8 \text{ s}^{-1}$ . Surface undulation typical of step-graded SiGe quantum wells (see Ref. [10]) gives  $D \approx 200 \text{ nm} \lesssim 15\lambda$ , though this interface imperfection is avoidable with heterostructures grown on defect-free nanomembrane substrates [26].

For a realistic cylindrical mpDBR cavity, the modes can be constructed as standing waves with energy  $\hbar\omega$ , and wave number  $q$  along the pillar  $z$ -direction, with stress-free boundary conditions on the cylindrical surface. The displacements for compressional modes (see e.g. Ref.[11]) are:  $u_r(r, z) = [A_r J_1(\eta_l r) + B_r J_1(\eta_t r)] \sin qz$ ,  $u_z(r, z) = [A_z J_0(\eta_l r) + B_z J_0(\eta_t r)] \cos qz$ , where  $J_{0,1}(r)$  are Bessels of 1st kind,  $\eta_{l,t} \equiv \sqrt{\omega^2/v_{l,t}^2 - q^2}$ , and  $A_i$ ,

$B_i$  are constants. These modes are lower in energy and couple strongly to the donor; the related strain has a node at the Si-cavity  $z$ -boundaries (for  $\lambda$ -cavity) [24]. For a fixed resonant frequency  $\omega$  and lateral size  $D$ , the dispersion relation  $q = \omega/v_q(D)$  has multiple solutions  $q_i, i = 0, 1, 2, \dots$ , where  $q_0$  stands for the fundamental mode,  $q_1$  for the 1st excited mode, etc. Each mode propagates with its own phase velocity  $v_{q_i}(D) \neq v_l, v_t$ . For a  $\lambda$ -cavity and  $D = \lambda_l$  we calculate via Eq.(1) maximal coupling to the fundamental mode with  $\lambda_{q_0} = 6.9$  nm to be  $g_{1\lambda}^{(0)} = g_{\max} = 6.5 \cdot 10^9 \text{ s}^{-1}$  (see Table I), comparable to the above estimation. For larger  $D$ , however, the coupling to the fundamental mode rapidly decreases (e.g.  $g_{5\lambda}^{(0)} = 5.8 \cdot 10^5 \text{ s}^{-1}$ ) since the mode transforms to a surface-like Rayleigh wave ( $v_{\text{Rayleigh}} < v_t$ ). Coupling to higher mode branches is appreciable and decreases roughly as  $1/\sqrt{V}$ , e.g., for the 1st mode branch,  $g_{1\lambda}^{(1)} = 2.4 \cdot 10^9 \text{ s}^{-1}$  and  $g_{5\lambda}^{(1)} = 3 \cdot 10^8 \text{ s}^{-1}$ . Among various mode choices we note that for any diameter  $D$  there is a higher excited mode with resonant wavelength close to that for longitudinal phonons. E.g., for  $D = 3\lambda_l$  we found the wavelength of the resonant 4<sup>th</sup> excited mode as  $\lambda_{q_4} \simeq 12.4 \text{ nm}$  and the coupling  $g_{3\lambda}^{(4)} = 3 \cdot 10^9 \text{ s}^{-1}$  (i.e., values similar to the rectangular DBR estimate).

*Loss.* Losses in this system are dominated by donor relaxation and leakage of the confined phonon mode. Similar to cQED (see, e.g., Ref. [3]), one can argue that the donor relaxation,  $\Gamma_{\text{relax}}$ , to modes different than the cavity mode (and generally not trapped into the cavity) is bounded by the donor spontaneous emission rate in the bulk:  $\Gamma_{\text{relax}} \lesssim \Gamma$ . We calculated the bulk donor relaxation to longitudinal and transverse phonons to be  $\Gamma_{ge}^{(l)} = 3 \cdot 10^7 \text{ s}^{-1}$  and  $\Gamma_{ge}^{(t)} = 9.2 \cdot 10^7 \text{ s}^{-1}$ , respectively, for the 3 meV transition ( $\Gamma = \Gamma_{ge}^{(l)} + \Gamma_{ge}^{(t)} = 1.2 \cdot 10^8 \text{ s}^{-1}$ ). The relaxation to photons is electric dipole forbidden and suppressed [15] by  $(\lambda_{\text{photon}}/a_B^*)^2 \sim 10^{10}$ .

The cavity mode loss rate is calculated as mainly due to leakage through the DBR mirrors, similar to optical DBR cavities [28] (except that for phonons there is no leakage through the sides). Generally, for the cylindrical micropillar DBRs, the cavity mode involves coupled propagation along the micropillar of two displacement components,  $u_z(r, z)$ ,  $u_r(r, z)$ , and two stress fields,  $T_{zz}$ ,  $T_{zr}$ . For small diameters,  $D \ll \lambda_l$ , the fundamental mode becomes mainly longitudinal ( $\sim u_z$ ), propagating with the Young velocity,  $v_0 = \sqrt{E/\rho}$ . Using  $4 \times 4$  transfer matrices we calculated  $Q_{\text{mpDBR}}^{(0)} \simeq 10^6$  for  $N = 33$  layers for the confined, mixed fundamental mode at  $D = \lambda_l$ , that is close to the limiting  $Q$ -factor related to pure longitudinal propagation[31]. (This is also similar to the 1D DBR value relevant for  $D \gg \lambda_l$ ). For our design we obtain a cavity loss rate  $\kappa = \Delta_v/\hbar Q \simeq 2.8 \cdot 10^6 \text{ s}^{-1}$ . This can be decreased by adding more layers.

At low temperatures the phonon anharmonicity losses are negligible (a rate  $\Gamma_{\text{anh}} \simeq 1.4 \cdot 10^4 \text{ s}^{-1}$  at 3 meV),

parameter	symbol	circuit-QED	P:Si/phonon	Li:Si/phonon
resonance freq.	$\omega_r/2\pi$	10 GHz	730 GHz	142 GHz
vac. Rabi freq.	$g/\pi$	100 MHz	2.1 GHz	13.8 MHz
cavity lifetime	$1/\kappa, Q$	160 ns, $10^4$	$0.22 \mu\text{s}, 10^6$	$1.1 \mu\text{s}, 10^6$
TLS lifetime	$1/\Gamma$	$2 \mu\text{s}$	8.2 ns	$22 \mu\text{s}$
critical atom #	$2\Gamma\kappa/g^2$	$\lesssim 6 \cdot 10^{-5}$	$\lesssim 3 \cdot 10^{-5}$	$\lesssim 4 \cdot 10^{-5}$
crit. phonon #	$\Gamma^2/2g^2$	$\lesssim 10^{-6}$	$\lesssim 2 \cdot 10^{-4}$	$\lesssim 6 \cdot 10^{-7}$
# Rabi flops	$2g/(\kappa+\Gamma)$	$\sim 100$	$\sim 102$	$\sim 93$

Table I. Key rates and parameters for circuit QED [33] (1D cavity) vs. the phonon system; we show calculations for maximal coupling for a  $\lambda$ -cavity with lateral diameter of  $D = \lambda_l$  (in general,  $g \sim 1/\sqrt{V}$ ),  $Q = 10^6$ , and comparable number of Rabi flops [37].

while scattering off impurity mass fluctuations in natural Si amounts to a rate two orders of magnitude larger:  $\Gamma_{\text{imp}} \approx 7 \cdot 10^5 \text{ s}^{-1}$ . It is notable that in isotopically purified bulk silicon (an enrichment of  $^{28}\text{Si}$  to 99%) the scattering rate will decrease by an order of magnitude and the related phonon mean free path will be of the order of  $v_l/\Gamma_{\text{imp}} \approx 10 \text{ cm}$  [11, 29, 32]. In this case, the cavity leakage dominates,  $\kappa \gg \{\Gamma_{\text{anh}}, \Gamma_{\text{imp}}\}$ , and the number of vacuum Rabi flops can reach as high as  $n_{\text{Rabi}} = 2g(D)/(\Gamma + \kappa) \simeq 102$  for a cavity  $Q$ -factor,  $Q = 10^6$ , and some  $n_{\text{Rabi}} \simeq 77$  for  $Q = 10^5$ . For  $D = 10\lambda_l$  and similar  $Q$  one still has:  $n_{\text{Rabi}}^{(1)} \simeq 1$  (17) for the 1st (2nd) excited mode. Further, nearby modes can be well separated from the resonant mode, e.g. for the fundamental mode and  $D = \lambda_l$  the next mode (in transverse direction) is  $\sim 0.3 \Delta_v = 0.9 \text{ meV}$  off; the transverse separation for  $D = 10\lambda_l$  (for the 1st excited mode) gives  $0.009 \Delta_v$ , which is more than two orders of magnitude larger than the linewidth  $\Gamma_0 \simeq (\Gamma + \kappa)/2$  of the two hybridized levels.

*Experiment and Discussion.* We have shown that the donor:Si cavity-phonon can enter the strong coupling regime with  $2g/(\Gamma + \kappa) \sim 10 - 100$  (Table I). A principle experimental confirmation would be the observation of the ‘‘vacuum’’ Rabi splitting:  $\Omega_0 = [g^2 - (\Gamma - \kappa)^2/4]^{1/2}$ ; two resolved spectral peaks can be observed if  $2\Omega_0 \geq \Gamma_0$ . The Rabi splitting can be enhanced as  $\Omega_0 \simeq g\sqrt{N}$  by placing more than one donor ( $N > 1$ ) in the cavity [1, 3] (e.g., via a delta-doped layer). This could allow for large coupling even for large diameter micropillars/ 1D DBR structures (since  $\frac{\sqrt{N}}{\sqrt{V}} \propto \frac{\sqrt{D^2}}{D} = 1$ ). Further, strain or electric field (from a top gate) [10, 34, 35] can be used to tune the valley transition into resonance.

Experimental techniques are available to probe the Si-phonon (low temperature,  $T \sim 1 \text{ K}$ , and low phonon numbers are assumed). First, free-electron lasers have been used to probe the  $1s - 2p$  transitions in P:Si [18]. Observation of the vacuum Rabi splitting is possible by measurement of the absorption spectrum of the allowed optically probed transition  $1s(T_2) \rightarrow 2p_0$  ( $\sim 30 \text{ meV}$ ) us-

ing weak optical excitation. Appropriate phonons can be introduced to the system by excited valley state emission, by piezo-actuators, or by increasing the temperature, as was done for the first observations of Rabi oscillations [36] (phonons of 3 meV  $\sim$  30 K). Second, pump and probe optical techniques have been demonstrated to observe coherent phonon effects in III-V [7, 13] and SiGe [20] SL heterostructures. Observing the reflected phonons from this structure will show the phonon-Rabi splitting characteristic of cavity-QED systems [1].

The cavity-phonon can be realized in other materials and systems. In particular, our system should be compatible with recently demonstrated (though in the few GHz range) high-Q phononic band-gap nano-mechanical and opto-mechanical (membrane) cavities in silicon (e.g., in [7] and [38]). Quantum dots, spin transitions, color centers in diamond, and other donors (particularly Li:Si [10]) may offer smaller resonance energies and correspondingly larger cavities (wavelengths) [32]. In the case of [001]-strained Si considered in this paper, the two lowest levels in Li possess essentially the same state structure as P:Si and approach a splitting of  $\Delta_{\text{Li}} = 0.586$  meV for high strain (from zero splitting at no strain). We calculate (see Table I) the corresponding Li:Si donor-phonon coupling for the  $D = \lambda_l$  (now  $\lambda_l = 63.2$  nm) reference cavity; strong coupling can still be reached. For the DBR cavities, the Si critical thickness can be made 80 – 100 nm by lowering the Ge content in the substrate. For 2D-phononic bandgap cavities, direct numerical calculations for cavity-trapped phonons ( $\omega_r/2\pi \approx 10$  GHz) in novel Si-nanostructures [38] show the potential to reach  $Q_{\text{cav}} \gtrsim 10^7$  in the ideal case.

The phonon is a new component for constructing and controlling macroscopic artificial quantum systems based on sound. Besides single phonon devices, systems composed of many coupled phonitons could exhibit novel quantum many-body behavior. For example, “solid-sound” systems in analogy with coupled cavity-QED solid-light systems [5] could demonstrate Mott insulator like states of phonons in coupled phonon cavities. Cavity/qubit geometries such as these may also be relevant for quantum computing (QC) applications: to mediate interactions between distant qubits or inhibit decoherence. The systems proposed here will benefit from the drive in silicon QC towards more purified materials, perfect surfaces, and precise donor placement.

*Acknowledgments.* Special thanks to Chris Richardson for input on realistic SiGe heterostructures and to Ari Mizel, Robert Joynt, and Mark Friesen for valuable discussion. This work was funded in part by DARPA.

Phys. **73**, 565-582 (2001).

- [3] Y. Yamamoto, F. Tassone, and H. Cao, *Semiconductor cavity Quantum Electrodynamics* (Springer, Berlin, 2000).
- [4] P. Littlewood, *Science* **316**, 989 (2007).
- [5] A. D. Greentree *et al.*, *Nature Physics* **2**, 856 (2006).
- [6] A. Kavokin and G. Malpuech, *Cavity Polaritons, v.32* (Elsevier, Amsterdam, 2003).
- [7] A. J. Kent *et al.*, *Phys. Rev. Lett.* **96**, 215504 (2006); C. A. Regal *et al.*, *Nature Physics* **4**, 555 (2008); M. Eichenfield *et al.*, *Nature* **462**, 78 (2009); A. K. Huttel *et al.*, *Nano Lett.* **9**, 2547 (2009); T. Rocheleau *et al.*, *Nature* **463**, 72 (2010); R. P. Beardsley *et al.*, *Phys. Rev. Lett.* **104**, 085501 (2010); A. D. O’Connell *et al.*, *Nature* **464**, 697 (2010); A. Bruchhausen *et al.* *Phys. Rev. Lett.* **106**, 077401 (2011).
- [8] A. Khaetskii, and Yu. Nazarov *Phys. Rev. B* **64**, 125316 (2001); C. Tahan, M. Friesen, and R. Joynt, *Phys. Rev. B* **66**, 035314 (2002); I. Wilson-Rae and A. Imamoglu, *Phys. Rev. B* **65**, 235311 (2002).
- [9] J. I. Cirac and P. Zoller, *Phys. Rev. Lett.* **74**, 4091 (1995).
- [10] V. N. Smelyanskiy, A. G. Petukhov, and V. V. Osipov, *Phys. Rev. B* **72**, 081304(R) (2005).
- [11] P. Rabl *et al.*, *Phys. Rev. B* **79**, 041302(R) (2009).
- [12] D. Porras and J. I. Cirac, *Phys. Rev. Lett.* **93**, 263602 (2004).
- [13] The *phoniton* involves a short-range electron-acoustic-phonon interaction (in a non-polar crystal). The term polaron has been reserved for a propagating electron plus the (long-range [2]) polarization field (usually optical phonons) in an ionic crystal.
- [14] G. L. Bir and G. E. Pikus, *Symmetry and Strain-induced Effects in Semiconductors* (IPST, Jerusalem; John Wiley & Sons, New York, 1974).
- [15] P. Yu and M. Cardona, *Fundamentals of Semiconductors* (Springer, Berlin, 2010).
- [16] D. Wilson and G. Feher, *Phys. Rev.* **124**, 1068 (1961).
- [17] T. G. Castner, *Phys. Rev.* **130**, 58 (1963).
- [18] P. T. Greenland *et al.*, *Nature* **465**, 1057 (2010).
- [19] M. Trigo *et al.*, *Phys. Rev. Lett.* **89**, 227402 (2002).
- [20] Y. Ezzahri *et al.*, *Phys. Rev. B* **75**, 195309 (2007).
- [21] K. Brunner, *Rep. Prog. Phys.* **65**, 27 (2002).
- [22] S. M. Rytov, *Akust. Zh.* **2**, 71 (1956) [*Sov. Phys. Acoust.* **2**, 68 (1956)].
- [23] S. M. Komirenko *et al.*, *Phys. Rev. B* **62**, 7459 (2000).
- [24] The intervalley transition  $1s(A_1) \rightarrow 1s(T_2)$  gives an odd in  $z$  contribution, Eq. (2), that overlaps with the strain, since at maximum  $\mathbf{u}(\mathbf{r})$  strain changes sign.
- [25] P. W. Leu, A. Svizhenko, and K. Cho, *Phys. Rev. B* **77**, 235305 (2008).
- [26] D. M. Paskiewicz *et al.*, *ACS Nano* **5** (7), 5814 (2011).
- [27] P. R. Berman, *Cavity Quantum Electrodynamics* (Academic Press, Boston, 1994).
- [28] M. Pelton *et al.*, *IEEE J. Quant. Electronics* **38**, 170 (2002).
- [29] K. Schwab *et al.*, *Nature* **404**, 974 (2000).
- [30] A. N. Cleland, *Foundations of Nanomechanics* (Springer, Berlin, 2003).
- [31] For 1D DBR cavity we evaluate:  $Q_{\text{DBR}} \simeq 2\pi(d_c + L_{\text{DBR}})\sqrt{R_c}/\lambda \ln R_c$ , where  $L_{\text{DBR}} = Z_A Z_B \lambda_q / 2Z_c |Z_B - Z_A|$  is the acoustic DBR mirror length and  $R_c = [(Z_s/Z_c - Z_r^{2N})/(Z_s/Z_c + Z_r^{2N})]^2$  is the peak power reflectivity for  $N$  layers with impedance ratio  $Z_r =$

[1] H. J. Kimble, *Physica Scripta* **T176**, 127 (1998).

[2] J.-M. Raimond, M. Brune, and S. Haroche, *Rev. Mod.*

$\rho_{AV_A}/\rho_{BV_B}$  ( $Z_s/Z_c$  are the impedances of the substrate/cavity respectively).

- [32] For long enough wavelengths one can neglect roughness effects in the phonon surface reflection as indicated in thermal conductance experiments. [11, 29].
- [33] A. Blais *et al.*, Phys. Rev. A **69**, 062320 (2004).
- [34] M. Friesen, Phys. Rev. Lett. **94**, 186403 (2005).
- [35] G. P. Lansbergen *et al.* Nature Phys. **4**, 656 (2008); L. Dreher *et al.* Phys. Rev. Lett. **106**, 037601 (2011).
- [36] G. Rempe, H. Walther, and N. Klein, Phys. Rev. Lett. **58**, 353 (1987).
- [37] For 3D-optical/microwave cavities [1, 2], the number of Rabi flops is limited by the finite transit time.
- [38] A.H. Safavi-Naeini and O. Painter, Optics Express **18**, 14926 (2010).

## SUPPLEMENTAL MATERIAL

### Deriving the phonon Hamiltonian

In semiconductors at low energies, the conduction band plays a role similar to the QED vacuum: the quasi-free electrons propagate according to a quadratic dispersion, scatter off acoustic phonons that possess linear dispersion, and can be bound to charged impurity potentials to establish hydrogen-like atoms (donors). Thus, the pattern of QED (matter and photon interactions) repeats itself in the behavior of electronic quasiparticles in the solid (the “matter”) and the phonon vibrations in a crystal (the “photons”). Consider the electron-phonon interaction. The Hamiltonian can be rearranged into the electron part  $H_e$ , the phonon part  $H_{\text{ph}}$ , and the electron-phonon interaction  $H_{e,\text{ph}}$ :  $H = H_e + H_{\text{ph}} + H_{e,\text{ph}}$ , where  $H_e = \frac{p^2}{2m} + V_{\text{lat}}(\mathbf{r})$  includes the periodic lattice potential  $V_{\text{lat}}(\mathbf{r})$  of the perfect crystal acting on an electron at point  $\mathbf{r}$ . For small atomic displacements  $\mathbf{u}(\mathbf{r})$  an expansion in normal modes gives

$$\mathbf{u}(\mathbf{r}) = \sum_{\mathbf{q},\sigma} (\mathbf{u}_{\mathbf{q}\sigma}(\mathbf{r}) b_{\mathbf{q}\sigma} + \mathbf{u}_{\mathbf{q}\sigma}^*(\mathbf{r}) b_{\mathbf{q}\sigma}^\dagger), \quad (\text{S1})$$

which approximately diagonalizes the phonon part  $H_{\text{ph}}$ :  $H_{\text{ph}} = \sum_{\mathbf{q},\sigma} \hbar\omega_{\mathbf{q}\sigma} (b_{\mathbf{q}\sigma}^\dagger b_{\mathbf{q}\sigma} + \frac{1}{2}) + H_{\text{anh}}$ . The small anharmonicity,  $H_{\text{anh}} = c b_{\mathbf{q}\sigma}^\dagger b_{\mathbf{q}'\sigma'} b_{\mathbf{k}\sigma} + \dots$ , is related to phonon self-interaction. The mode normalization in Eq. S1 is  $\int d^3\mathbf{r} \mathbf{u}_{\mathbf{q}\sigma}^*(\mathbf{r}) \mathbf{u}_{\mathbf{q}\sigma}(\mathbf{r}) = \frac{\hbar}{2\rho\omega_{\mathbf{q}\sigma}}$ , so that  $b_{\mathbf{q}\sigma}^\dagger$  creates a phonon in the mode  $\mathbf{q},\sigma$  with energy  $\hbar\omega_{\mathbf{q}\sigma}$  in a material with mass density  $\rho$ . The vector  $\mathbf{q}$  denotes a collective index of the discrete phonon mode defined via the phonon cavity boundary conditions and quantization volume  $\mathcal{V}$ . In particular, the plane wave expansion corresponds to rectangular periodic boundary conditions and  $\mathbf{u}_{\mathbf{q}\sigma}(\mathbf{r}) = \left(\frac{\hbar}{2\rho\mathcal{V}\omega_{\mathbf{q}\sigma}}\right)^{1/2} \boldsymbol{\xi}_{\mathbf{q},\sigma} e^{-i\mathbf{q}\cdot\mathbf{r}}$  with wave vector  $\mathbf{q}$ , polarization  $\boldsymbol{\xi}_{\mathbf{q},\sigma}$ , and phonon branch  $\sigma$ .

By considering low-energy acoustic phonons for electrons close to the band minimum,  $\mathbf{k} \approx \mathbf{k}_0$ , the electron-phonon interaction can be written as

$$H_{e,\text{ph}}^{\text{ac}}(\mathbf{r}) = \sum_{ij} D_{ij} \varepsilon_{ij}(\mathbf{r}). \quad (\text{S2})$$

The operator  $D_{ij} = -\hat{p}_i \hat{p}_j / m + V_{ij}(\mathbf{r})$  (with  $\hat{\mathbf{p}} = -(i/\hbar)\nabla$  and a crystal model dependent  $V_{ij}(\mathbf{r})$ ) coincides with the constant-strain deformation potential [1, 2] and the strain  $\varepsilon_{ij}(\mathbf{r}) = \frac{1}{2} \left( \frac{\partial u_i}{\partial r_j} + \frac{\partial u_j}{\partial r_i} \right)$  causes transitions between electronic states. A donor impurity center makes a perturbation to the perfect crystal, thus binding the low-energy electrons. One introduces electron field operators  $\Psi(\mathbf{r}) = \sum_s c_s \psi_s(\mathbf{r})$  related to the donor bound states  $\psi_s(\mathbf{r})$ , where  $c_s$  is the annihilation operator for that state. By integrating Eq. (S2) over the charge

density operator,  $\Psi^\dagger(\mathbf{r})\Psi(\mathbf{r})$ , the electron-phonon interaction takes the second-quantized form:  $H_{e,\text{ph}} = \sum_{s,s'} \sum_{\mathbf{q},\sigma} c_{s'}^\dagger c_s (b_{\mathbf{q},\sigma} + b_{\mathbf{q},\sigma}^\dagger) V_{\mathbf{q},\sigma}^{s's}$  where the matrix element,  $V_{\mathbf{q},\sigma}^{s's} = \langle \psi_{s'}; \{\mathbf{q},\sigma\} | H_{e,\text{ph}}^{\text{ac}} | \psi_s \rangle$ , describes phonon transitions between the bound states.

Similar to quantum optics, the electron-phonon interaction  $H_{e,\text{ph}}$  describes transitions in an  $n$ -level atom (although the analog of electric-dipole approximation is not made). The Jaynes-Cummings type Hamiltonian [3] results when a *single* phonon mode  $\mathbf{q}$  is in resonance with the transition (i.e.,  $\omega_{\mathbf{q},\sigma} \approx \omega_{ss'}$ ). This is possible if we have a suitable phononic cavity and the phononic bandwidth  $\Delta\omega_{\mathbf{q}}$  is much smaller than the transition frequency  $\omega_{ss'}$ . Introducing rising (lowering) operators  $\sigma^+ = c_{s'}^\dagger c_s$  ( $\sigma^- = c_s^\dagger c_{s'}$ ) for the specified transition ( $s \rightarrow s'$ ) and supposing real matrix elements such that  $V_{\mathbf{q},\sigma}^{s's} = V_{\mathbf{q},\sigma}^{ss'} \equiv \hbar g_{\mathbf{q}}$ , we obtain  $H_g = \hbar g_{\mathbf{q}} (\sigma^+ + \sigma^-) (b_{\mathbf{q},\sigma} + b_{\mathbf{q},\sigma}^\dagger)$ . In the typical case of  $g_{\mathbf{q}} \ll \omega_{ss'}$  only the “energy conserving” operators  $\sigma^+ b_{\mathbf{q},\sigma}$ ,  $\sigma^- b_{\mathbf{q},\sigma}^\dagger$  will survive in the rotating wave approximation obtaining  $H_g \approx H^{\text{JC}} = \hbar g_{\mathbf{q}} (\sigma^+ b_{\mathbf{q},\sigma} + \sigma^- b_{\mathbf{q},\sigma}^\dagger)$ . The total Hamiltonian in such a cavity approximation can then be written as

$$H = \hbar\omega_{\mathbf{q},\sigma} \left( b_{\mathbf{q},\sigma}^\dagger b_{\mathbf{q},\sigma} + \frac{1}{2} \right) + \frac{\hbar\Delta}{2} \sigma_z + H_g + H_\kappa + H'_{\text{anh}} + H_\Gamma, \quad (\text{S3})$$

where we have denoted the atom transition frequency as  $\Delta \equiv \omega_{ss'}$ .

### Phonon-donor coupling

For shallow donors the wave function is localized in “valleys” in  $k$ -space, near the local conduction band minima  $\mathbf{k}_j$ , and for Si (tetrahedral symmetry) these are displaced at  $k_0 \simeq 0.85 2\pi/a_0$  along the equivalent directions  $\hat{x}$ ,  $-\hat{x}$ ,  $\hat{y}$ ,  $-\hat{y}$ ,  $\hat{z}$ ,  $-\hat{z}$  in the cubic lattice. The valley state is a modulated Bloch wave:  $\psi_s^j(\mathbf{r}) \approx \psi_{\mathbf{k}_j}(\mathbf{r}) \Phi_s^j(\mathbf{r})$  with the well known envelope functions  $\Phi_s^j(\mathbf{r})$  [4]. Each donor bound state is superpositions of such valley states,  $\psi_s(\mathbf{r}) = \sum_{j=1}^6 \alpha_j^s \psi_s^j(\mathbf{r})$  with  $\alpha_j^s$  being the “valley populations”. The six-fold degeneracy of conduction electrons in silicon is broken both by strain (e.g., due to the lattice mismatch with a  $\text{Si}_{1-x}\text{Ge}_x$  substrate) and the sharp potential of the phosphorous (or other) donor. Thus the two lowest states in our device approach symmetric and antisymmetric combinations of the  $\pm z$  valley states (see Fig. 1, main text) [5] and asymptote to  $E_{s's} = E_e - E_g \simeq 3.02 \text{ meV}$  splitting for large ( $x \gtrsim 0.1$ ) mismatch. Both states are “s-like”, having the same s-like envelope function but opposite parity due to different content of the highly oscillating Bloch components. The next highest state is “p-like” and lies some 30 meV above the ground state.

One can calculate the partial matrix element for intervalley transitions in the long wave-length (acoustic) limit [4, 6]:

$$\begin{aligned}
V_{ij}^{s's}(\mathbf{q}, \sigma) &= \left( \frac{\hbar}{2\rho\mathcal{V}\omega_{\mathbf{q},\sigma}} \right)^{1/2} \\
&\times \left( \Xi_d(\mathbf{q}\xi_{\mathbf{q},\sigma}) + \frac{1}{2}\Xi_u \left\{ (\mathbf{q}\hat{\mathbf{k}}_i)(\xi_{\mathbf{q},\sigma}\hat{\mathbf{k}}_i) + (\mathbf{q}\hat{\mathbf{k}}_j)(\xi_{\mathbf{q},\sigma}\hat{\mathbf{k}}_j) \right\} \right) \\
&\times \sum_{\mathbf{G}} a_{\mathbf{G}}^{ij} \int d\mathbf{r} [\Phi_{s'}^i(\mathbf{r})]^* \Phi_s^j(\mathbf{r}) e^{-i(\mathbf{k}_i+\mathbf{q}+\mathbf{G}-\mathbf{k}_j)\mathbf{r}}. \quad (\text{S4})
\end{aligned}$$

The total matrix element is given by a sum over all valley contributions weighted by the valley populations:  $V_{\mathbf{q},\sigma}^{s's} = \sum_{i,j} \alpha_i^{s'} \alpha_j^s V_{ij}^{s's}(\mathbf{q}, \sigma)$ . Here,  $\Xi_d$  and  $\Xi_u$  are the low- $\mathbf{q}$  deformation potentials (that compose  $D_{ij}$  in Eq. S2),  $\hat{\mathbf{k}}_i$  is a unit vector towards the  $i$ th valley (e.g.  $\hat{\mathbf{k}}_1 = \hat{x}$ ,  $\hat{\mathbf{k}}_2 = -\hat{x}$ , etc.), and  $a_{\mathbf{G}}^{ij}$  are the Fourier series expansion coefficients of the function  $u_{\mathbf{k}_i}^*(\mathbf{r})u_{\mathbf{k}_j}(\mathbf{r})$  ( $u_{\mathbf{k}}$  are the periodic parts of the Bloch waves), i.e.  $u_{\mathbf{k}_i}^*(\mathbf{r})u_{\mathbf{k}_j}(\mathbf{r}) = \sum_{\mathbf{G}} a_{\mathbf{G}}^{ij} e^{-i\mathbf{G}\mathbf{r}}$ . In the sum over  $\mathbf{G}$  the main contribution comes from the minimal reciprocal vectors. Higher terms are suppressed due to spatial confinement of the orbital part and/or rapid decreasing of the Fourier coefficients  $a_{\mathbf{G}}^{ij}$  for higher  $\mathbf{G}$  [7]. Due to different parity of the valley populations under inversion  $\mathbf{k}_{\hat{z}} \rightarrow \mathbf{k}_{-\hat{z}}$  the intravalley contributions ( $i = j$ ) will cancel. Leading contribution to  $V_{\mathbf{q},\sigma}^{s's}$  comes from intervalley (Umklapp) transitions with  $\mathbf{q} \approx \mathbf{q}_u \equiv \mathbf{G}_{\pm 1} - 2\mathbf{k}_{\hat{z}}$ , where  $\mathbf{G}_{\pm 1} = \frac{4\pi}{a_0}(0, 0, \pm 1)$  is the reciprocal vector along the  $\hat{z}$ -direction [6].

### Donor relaxation

The total emission rate is calculated from Eq. (S4) via the Golden Rule:  $\Gamma_{ge}^{(\sigma)} = \sum_{\mathbf{q}} \frac{2\pi}{\hbar^2} |V_{\mathbf{q},\sigma}^{ge}|^2 \delta(\omega_{\mathbf{q},\sigma} - \omega_{ge})$ . Using the notations  $x \equiv \cos\theta$ ,  $J(x; \beta_q, \gamma_q) \equiv \frac{\alpha_q^2}{2\beta_q} I^{\text{ge}}(x)$  (cf. Eq. 2 of the main text), and  $\Xi^{(1)}(x) \equiv \Xi_d + \Xi_u x^2$ ,  $\Xi^{(t)}(x) \equiv \Xi_u x \sqrt{1-x^2}$  we obtain the emission rates for acoustic modes:

$$\begin{aligned}
\Gamma_{ge}^{(\sigma)} &= \frac{(bq_u)^2 \omega_{ge}^5 b^2}{4\pi\rho\hbar v_{\sigma}^7} \frac{|a_G|^2}{\left[1 + \frac{1}{4}(q^2 a^2 + q_u^2 b^2)\right]^6} \\
&\times \int_{-1}^1 dx [\Xi^{(\sigma)}(x) J(x; \beta_q, \gamma_q)]^2 \Big|_{q=q_{ge}^{(\sigma)}}, \quad (\text{S5})
\end{aligned}$$

where  $v_{\sigma}$  is the speed and  $q_{ge}^{(\sigma)} = \omega_{ge}/v_{\sigma}$  is the wave number of the emitted phonon of polarization  $\sigma$ . We mention that  $\Gamma_{ge}^{(\sigma)}$  as a function of energy of the transition must experience a maximum when  $q_{ge}^{(\sigma)}$  is close to the Umklapp value  $q_u$  or  $\frac{E_{ge}}{\hbar v_{\sigma}} \approx 0.3 \frac{2\pi}{a_0}$ . This corresponds to transition energies 19.2 meV and 13.3 meV for longitudinal and transverse phonons respectively, which is in accordance with Eq. (S5). Using the mass density

$\rho = 2330 \text{ kg m}^{-3}$  for Si and the deformational potential constants:  $\Xi_u(\text{Si}) \simeq 8.77 \text{ eV}$ ,  $\Xi_d(\text{Si}) \simeq 5.0 \text{ eV}$ , and  $a_G \approx 0.3$  [7] one obtains the rates at 3 meV:

$$\Gamma_{ge}^{(l)} = 3 \cdot 10^7 \text{ s}^{-1}, \quad \Gamma_{ge}^{(t)} = 9.2 \cdot 10^7 \text{ s}^{-1}. \quad (\text{S6})$$

For reference, the values calculated in the dipole approximation are about  $\approx 35 - 50\%$  larger than the above.

### Cavity design and cavity quality factors

#### 1D DBR cavity

Due to the analogy between light and sound in solids, the theory of optical DBRs can be applied to the design of acoustic DBRs. For acoustic waves propagating perpendicularly to the 1D DBR SL mirror, Bragg type interference leads to forming of frequency stop-bands [8] in the reflectivity spectrum, positioned around a central frequency (for the  $m^{\text{th}}$ -order band)  $\omega_m = m\pi(d_A/v_A + d_B/v_B)^{-1}$ . The presence of a resonant Si-cavity (a ‘‘defect’’) in the SL leads to a dip in the reflectivity spectrum (cf. Fig. 2), whose width would represent the 1D DBR  $Q$ -factor, providing the cavity losses are mainly through the DBR mirrors. Similar to optics, the transfer matrix method (see, e.g., Ref. [9]) allows us to evaluate  $Q_{\text{DBR}} \simeq 2\pi(d_c + L_{\text{DBR}})\sqrt{R_c}/\lambda \ln R_c$ , where  $L_{\text{DBR}} = Z_A Z_B \lambda_q / 2Z_c |Z_B - Z_A|$  is the acoustic effective DBR mirror length and  $R_c = [(Z_s/Z_c - Z_r^{2N})/(Z_s/Z_c + Z_r^{2N})]^2$  is the DBR peak power reflectivity calculated for  $N$  layers with layer impedance ratio  $Z_r = \rho_A v_A / \rho_B v_B$  ( $Z_s/Z_c$  are the impedances of the substrate/cavity respectively).

The cavity quality factor extracted numerically from the linewidth of the reflectivity dip (see Fig. 2) agrees well with the simple analytics. For our design, we choose the layer materials  $A = \text{Si}_{0.45}\text{Ge}_{0.55}$  and  $B = \text{Si}_{0.95}\text{Ge}_{0.05}$  with thicknesses of  $d_A = 2.1 \text{ nm}$  and  $d_B = 2.8 \text{ nm}$  (strain matched [10] to a substrate of  $\text{Si}_{0.74}\text{Ge}_{0.26}$ ), to confine a longitudinal phonon ( $d_c = \lambda_l$ ); we obtain a  $Q$ -factor of  $\sim 1.2 \cdot 10^5$  for  $N = 29$  SL layers; for  $N = 36$   $Q_{\text{DBR}}$  reaches  $10^6$ .

#### Micro-pillar DBR cavity

While longitudinal and transverse phonons formally decouple under isotropic approximation in the bulk, they combine in mpDBR cavity/waveguide modes due to the strong effect of the side boundaries, and propagate with a differing phase velocity  $v_q \neq v_l, v_t$ . For the cylindrical mpDBR cavity we focus on compressional modes only, since flexural modes are energetically higher, while torsional (transverse) modes do not couple to the donor. The boundary condition on the mpDBR cavity



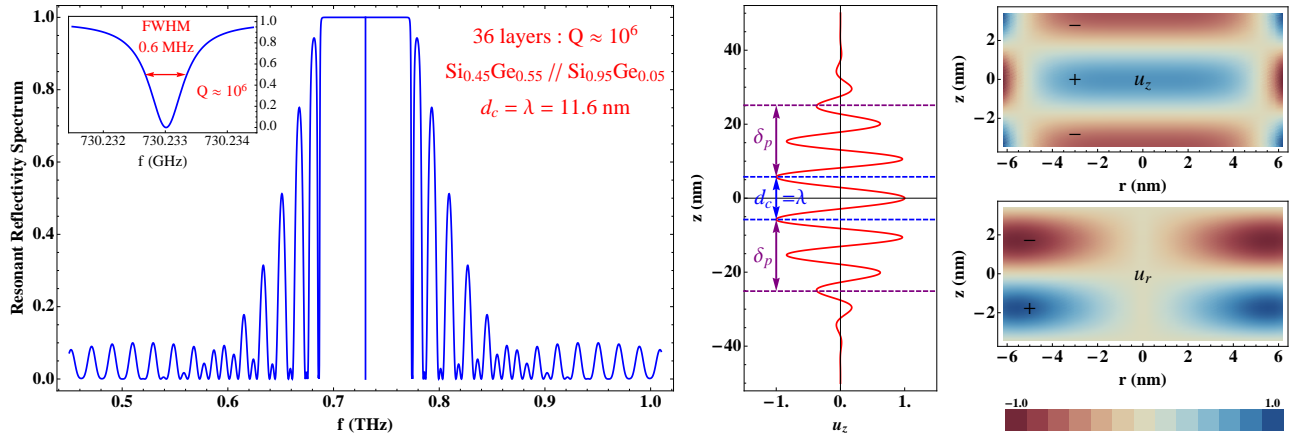


Figure 2. Reflectivity and field distribution of acoustic distributed Bragg reflector (DBR) phonon cavity. (left) Reflectivity spectrum of the phonon cavity enclosed by DBRs consisting of  $N = 36$  subsequent layers of thicknesses  $d_A \simeq 2.1$  nm/ $d_B \simeq 2.8$  nm ( $A = \text{Si}_{0.45}\text{Ge}_{0.55}/B = \text{Si}_{0.95}\text{Ge}_{0.05}$ ). Slight thickness changes due to finite interlayer spacing approximation do not cause significant change in  $Q$ . For the 1D calculations we use the [001] phonon velocity of  $v_l = 8.43 \cdot 10^3$  m/s giving  $\lambda_l \simeq 11.6$  nm. The sharp dip in the reflectivity at  $f_0 = 0.73$  THz corresponds to the donor transition energy  $\sim 3$  meV. The left inset shows a zoom in of the reflectivity dip and corresponds to the confined cavity mode with FWHM of 0.6 MHz and  $Q \approx 10^6$ . (middle) Amplitude of the localized phonon displacement in the 1D DBR cavity is shown with respect to the position along [001] in Si, with the Si cavity of thickness  $d_c$  and penetration depth  $\delta_p$  into the DBR, respectively. (right) The mixed phonon mode in a 3D micro-pillar DBR structure. Normalized amplitudes of the phonon displacements  $u_z(r, z)$  and  $u_r(r, z)$  are shown for the fundamental mode inside the Si cavity of thickness 6.9 nm and diameter  $D = 12.3$  nm. The DBR mirrors enclosing the Si cavity are constructed from alternating layers of  $\text{Si}_{0.95}\text{Ge}_{0.05}/\text{Si}_{0.45}\text{Ge}_{0.55}$  with thicknesses of 1.7/1.2 nm, respectively. 3D cavity reflectivity spectrums are qualitatively similar to the 1D case.

$z$ -interfaces is linked to the Bragg resonance condition at the first zone center stop band (for  $\lambda_q$ -cavity), leading to  $q = 2\pi/d_c = \Delta_v/\hbar v_q$ , where  $q$  is the cavity phonon wave vector along the pillar  $z$ -axis. Additionally, the free-standing (stress-free) boundary condition along the cylindrical surface implies for the stresses:  $T_{rr} = T_{rz} = 0$  at  $r = R$ , and leads to the well-known Pochhammer-Chree dispersion relation of compressional waves (see, e.g., Ref. [11]),  $2\eta_l(\eta_t^2 + q^2)J_1(\eta_l R)J_1(\eta_t R)/R - (\eta_t^2 - q^2)^2 J_0(\eta_l R)J_1(\eta_t R) - 4q^2\eta_l\eta_t J_1(\eta_l R)J_0(\eta_t R) = 0$ , where  $J_{0,1}(r)$  are Bessels of 1st kind,  $R = D/2$  is the radius, and  $\eta_l = \sqrt{\omega^2/v_l^2 - q^2}$ ,  $\eta_t = \sqrt{\omega^2/v_t^2 - q^2}$  may be interpreted as transverse wave vector components. For fixed  $\omega$ ,  $D$ , the dispersion relation possesses multiple solutions  $q_i = \omega/v_{q_i}(D)$ ,  $i = 1, 2, \dots$ . Each mode branch defines its own phase velocity  $v_{q_i}$ ,  $v_{q_0} < v_{q_1} < \dots$  with the fundamental mode branch having the smallest velocity.

The modes in the mpDBR cavity can be constructed as standing waves using waveguide solutions for compressional modes:

$$u_r(\mathbf{r}) = -A\eta_l \left[ J_1(\eta_l r) + \frac{2q^2}{\eta_t^2 - q^2} \frac{J_1(\eta_l R)}{J_1(\eta_t R)} J_1(\eta_t r) \right] \sin qz$$

$$u_z(\mathbf{r}) = Aq \left[ J_0(\eta_l r) - \frac{2\eta_l\eta_t}{\eta_t^2 - q^2} \frac{J_1(\eta_l R)}{J_1(\eta_t R)} J_0(\eta_t r) \right] \cos qz.$$

The relevant strain components have  $\sim \sin qz$  dependence, i.e., the strain has a node at the Si-cavity  $z$ -boundaries to ensure non-zero coupling with the donor  $A_1 \leftrightarrow T_2$  transition (see Eq. 2 of the main text).

The constant  $A$  can be calculated from a proper normalization condition:

$$\int_{V_{\text{cav}}} d^3\mathbf{r} \mathbf{u}_q^*(\mathbf{r}) \mathbf{u}_q(\mathbf{r}) = \gamma \frac{\hbar}{2\rho\omega q}, \quad (\text{S7})$$

where  $\mathbf{u}_q(\mathbf{r}) = \mathbf{e}_r u_r(r, z) + \mathbf{e}_z u_z(r, z)$  is the displacement “vacuum field” (see Eq. S1) in the Si-cavity. Here  $\gamma$  is the fraction of the phonon vacuum energy,  $\hbar\omega q/2$ , stored in the cavity of length  $d_c$ , while an energy fraction  $1 - \gamma$  is stored in the DBR mirrors, related to the penetration depth  $\delta_p$  shown on Fig. 2. Approximate transfer matrix calculations based on the propagation of four fields (the displacements  $u_z$ ,  $u_r$ , and the stresses  $T_{zz}$ ,  $T_{zr}$ ) along the mpDBR waveguide give  $\gamma \approx 0.3$  (note that the coupling  $g$  scales as  $\sim \sqrt{\gamma}$  which renormalizes the  $g_{max}$ ’s calculated in the text) that is commensurate with the value estimated from the 1D DBR field distribution.

For each mode of mpDBR considered in resonance with the donor, a suitable cavity design with appropriate cavity design parameters, i.e. cavity and SL layer thicknesses, strain matched substrate Ge content, etc. is required. In accordance with our 1D DBR design, layer materials  $A$  and  $B$  are kept the same. For a diameter of  $D = \lambda_l = 12.3$  nm, a Si-cavity thickness of  $d_c = \lambda_{q_0} = 6.9$  nm results with the fundamental mode being in resonance with the P donor (the layer thicknesses are correspondingly  $d_A = 1.7$  nm and  $d_B = 1.2$  nm). Using the TM method, the ideal  $Q$ -factor of the fundamental mode is calculated to range from  $10^4 - 10^6$  for



$N = 20 - 33$  unit layers of the DBR, and similar numbers appear for the higher excited modes.

### Anharmonicity and scattering off impurities

In isotropic crystals at low temperatures ( $T \ll \hbar\omega/k_B$ ) a TA-phonon decay is forbidden, while the LA-phonon decays through  $LA \rightarrow TA + TA$  and  $LA \rightarrow TA + LA$  channels. For Si,  $\Gamma_{LA}^{\text{tot}} \approx 4.5 \cdot 10^4 \nu_{\text{THz}}^5$  [12]; this gives for 3 meV (0.73 THz) a rate  $1.4 \cdot 10^4 \text{ s}^{-1}$  (Si anisotropy lifts out the TA selection rule, leading to same order of magnitude TA-decay rate; see, however, [12]). For larger temperatures ( $T \gtrsim 3\text{meV}/k_B \sim 30 \text{ K}$ ),  $\Gamma_{LA}$  scales as  $\omega T^4$  (Landau-Rumer effect, see e.g., Ref. [11]) leading to an order of magnitude enhancement. Stronger phonon losses come from scattering from isotopic point defects. For natural Si the isotope mass fluctuations lead to a rate  $\Gamma_{\text{imp}} \approx 2.43 \cdot 10^6 \nu_{\text{THz}}^4$  [12], which gives  $\sim 7 \cdot 10^5 \text{ s}^{-1}$  for 0.73 THz. The estimated rate gives a phonon mean free path of the order of  $v_l/\Gamma_{\text{imp}} \sim 1.2 \text{ cm}$ . An enrichment of  $^{28}\text{Si}$  to 99% (natural abundance of  $^{28}\text{Si}$  is 92.23%) decreases the scattering rate by one order of magnitude; so, the dominating phonon loss may become scattering off the surfaces and interfaces of the phonon microcavity [14].

In Ref. [15] via direct measurement of the phonon decay rate in a GaInAs SL cavity ( $\nu_1 = 0.46 \text{ THz}$ ):  $\Gamma_{\text{ph}} \simeq \Gamma_{\text{conf}} + \Gamma_{\text{anh}}$ , an anharmonicity rate was estimated as  $\Gamma_{\text{anh}} \simeq 3.3 \cdot 10^9 \text{ s}^{-1}$ , taking into account the phonon confinement due to the SL DBRs. The observed large rates are nevertheless in qualitative agreement with the above theoretical estimations, since the experiment was

performed at a high (room) temperature and dealt with large number of initially injected phonons [11]. Thus, we expect that in quantum-limited experiments at low temperatures ( $\sim 1 \text{ K}$ ) and low phonon occupation numbers scattering rates of the order of  $10^4 - 10^5 \text{ s}^{-1}$  can be achieved.

- 
- [1] C. Herring and E. Vogt, Phys. Rev. **101** 944 (1956).
  - [2] G. L. Bir and G. E. Pikus, *Symmetry and Strain-induced Effects in Semiconductors* (IPST, Jerusalem; John Wiley & Sons, New York, 1974).
  - [3] P. R. Berman, *Cavity Quantum Electrodynamics* (Academic Press, Boston, 1994).
  - [4] W. Kohn and J. M. Luttinger, Phys. Rev. **98** 915 (1955).
  - [5] D. Wilson and G. Feher, Phys. Rev. **124**, 1068 (1961).
  - [6] T. G. Castner, Phys. Rev. **130**, 58 (1963).
  - [7] B. Koiller, R. Capaz, X. Hu, and S. Das Sarma, Phys. Rev. B **70**, 115207 (2004).
  - [8] S. M. Rytov, Akust. Zh. **2**, 71 (1956) [Sov. Phys. Acoust. **2**, 68 (1956)].
  - [9] A. Kavokin and G. Malpuech, *Cavity Polaritons, v.32* (Elsevier, Amsterdam, 2003).
  - [10] K. Brunner, Rep. Prog. Phys. **65**, 27 (2002).
  - [11] A. N. Cleland, *Foundations of Nanomechanics* (Springer, Berlin, 2003).
  - [12] H. J. Maris and S.-I. Tamura, Phys. Rev. B **47**, 727 (1993).
  - [13] M. Trigo A. Bruchhausen, A. Fainstein, B. Jusserand, and V. Thierry-Mieg, Phys. Rev. Lett. **89**, 227402 (2002).
  - [14] M. Trigo, T. A. Eckhause, M. Reason, R. S. Goldman, and R. Merlin, Phys. Rev. Lett. **97**, 124301 (2006).
  - [15] M. F. Pasqual-Winter, G. Rozas, A. Fainstein, B. Jusserand, B. Perrin, A. Huynh, P. O. Vaccaro, and S. Saravanan, Phys. Rev. Lett. **98**, 265501 (2007).